Supplementary Information

Gradient fluorinated alloy to enable highly reversible Zn-metal anode chemistry

Guojin Liang[1], Jiaxiong Zhu[1], Boxun Yan[2], Qing Li[1], Ao Chen[1], Ze Chen[1], Xiaoqi Wang[3], Bo Xiong[3], Jun Fan[1], Xu Jin[3]*, Chunyi Zhi[1,4]*

[1]Department of Materials Science and Engineering, City University of Hong Kong, 83 Tat Chee Avenue, Kowloon, China

[2]Department of Electrical Engineering, City University of Hong Kong, Kowloon, Hong Kong, 999077, China

[3]China Research Institute of Petroleum Exploration & Development (RIPED), Petro China Research Center of New Energy, No. 20 Xueyuan Road Haidian District, Beijing, 100083, P. R. China

[4]Center for Advanced Nuclear Safety and Sustainable Development, City University of Hong Kong, Kowloon, Hong Kong, 999077, China

*Email: jinxu@petrochina.com.cn ; cy.zhi@cityu.edu.hk

Methods

Materials and preparations. Zn foils of 50 μm thickness was first washed in deionized (DI) water and ethanol for three times. Then, 0.2 g CuF_2 (Aladdin-C189213) was dissolved into DI water and the Zn foil was immersed in the CuF_2 solution for different time durations for 2, 5, 10 mins, respectively. The processed Zn foil was then rinsed with DI water and dried under vacuum at 60 °C for 4 hours and cut into 12 mm circular disc for investigation in coin cells. To realize large utilization ratio of Zn anode, Zn foils of 30 μm thickness were treated with the same procedure for the pouch cell.

I_2 cathode fabrication. First, activated carbon (AC) was first coated on the titanium mesh as hosting materials by mixing well with acetylene black (AB) and polyvinylidene difluoride (PVDF) in *N*-methylpyrrolidone (NMP) solvent with weight ratios of AC:AB:PVDF of 8:1:1, while the loading mass of AC is 10 mg cm^{-2}. Then, the I_2 electrode was electrodeposited to the large sized AC substrate (8 cm *8 cm) in solution of 1 M KI and 0.2 M $ZnSO_4$ under constant current of 100 mA, where the average areal capacity of iodine was designated at 3 mAh cm^{-2}. After I_2 deposition, it was washed with DI water and then dried in oven at 40 °C to serve as cathode in I_2-Zn cell. The I_2 electrode was cut into 12 mm circular disc for I_2-Zn coin cell, while two designed sized I_2 electrode (4.5 cm*5.8 cm) to individually face two sides of the GFA-Zn for I_2-Zn pouch cells to obtain a bipolar cell.

Electrochemical characterization. Symmetric cells and full cells were assembled using both bare Zn and GFA-coating protected Zn as anodes in CR-2032 coin cells, while the a volume of 100 μL of electrolyte (1 M $ZnSO_4$) was utilized with the glass fiber (Waterman-1820) as separator. The galvanostatic charging–discharging processes based on different current densities from 0.5 to 10 mA cm^{-2} were conducted using the CT2001A Battery Cycler (Wuhan, China). Cyclic voltammetry and Tafel plot were measured using a CHI-760 electrochemical working station. EIS measurement was conducted with a 5 mV amplitude AC signal with frequency ranging from 100 kHz to 0.1 Hz. The transference number is calculated by a current-time curve under potentiostatic polarization at 5 mV for 1000 seconds. Electronic resistivity of the GFA-coating layers was measured by examining the voltage response to a direct current (2 mA) on the cells with the bare Zn or GFA-5 electrode sandwiched between two stainless steel blocking electrodes.

Material characterizations. The electrodes were characterized with XRD (Bruker D2 Phaser), XPS (PHI Model 5802), Raman (PerkinElmer Raman 400F Spectrometer), SEM (ESEM, FEI/Philips XL30). As for the etching process of XPS measurement, the etched depth after 10 mins is estimated to be less than 0.3 μm, where the etching depth is 0.48 nm/s calibrated based on the reference Ta_2O_5 etching results. The specific surface area was measured by Brunauer-Emmett-Teller (BET) with N_2 adsorption-desorption measurements (Micromeritics, ASAP 2020) based on the Zn foil and GFA-Zn foil with size as 5 cm * 5 cm. The roughness of the surface coating is characterized by a laser scanning confocal microscope (VK-X1000, KEYENCE). The modulus mapping were measured by atomic force microscope (Bruker, DIMENSION ICON) and conducted in the quantitative nano mechanics mode (QNM), while the Young's modulus is obtained by fitting the curve using the Derjaguin–Muller–Toropov (DMT) model. The air pressure test is based on a sealed chamber home-designed, and a barometer is used to detect the change in air pressure during symmetric cell cycling. Changes in air pressure are finally converted into changes in mass corresponding to the produced H_2.

Field simulation

The simulation of the electric field and ion diffusion and drift was implemented in finite element solver. The domain of interest has a preset applied normalized voltage of 1 V with area of 50 μm $\times$ 50 μm. The electric potential was plotted by solving the Poisson equation in free space with floating potential for the artificial elements of GFA-particles. The ion diffusion and drifting was solved in the following method.

Given an ion flux of $N = D\nabla c - \mu c\nabla\phi$, where D is the ion diffusion constant, c is the concentration, μ is the ionic mobility, ϕ is the potential solved above, the drift-diffusion model can be presented by

$$\frac{\partial c}{\partial t} = -\nabla \cdot N$$

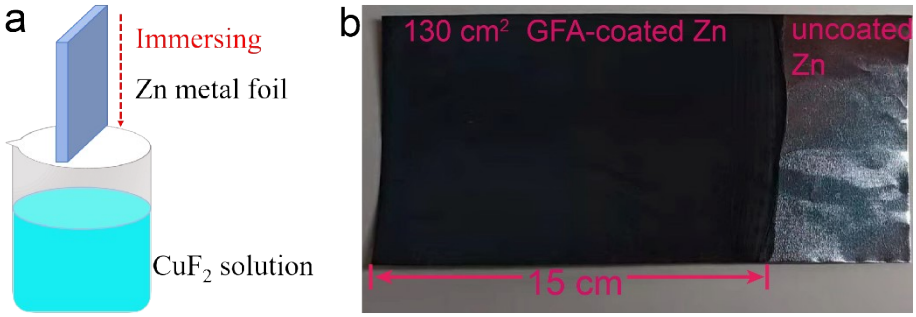

Figure S1. Schematic diagram of preparing GFA-coated Zn, with different soaking time durations. (B) A photo of a large sized as-obtained GFA-coated Zn reached about 130 cm^{-2}.

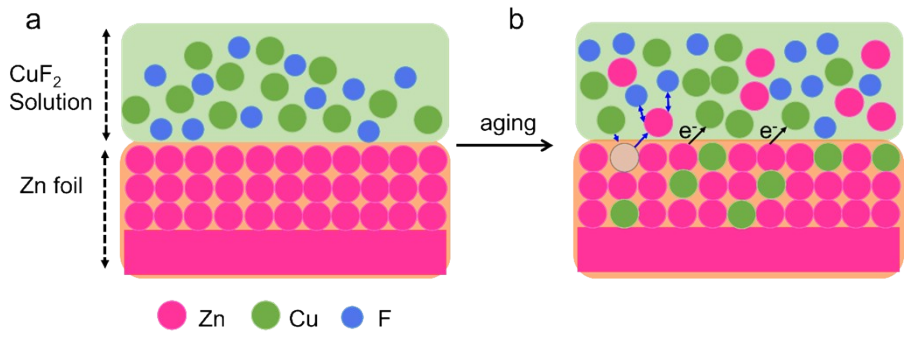

Figure S2. (a) Illustration of the initial state to observe the interface between Zn foil and CuF_2 solution. (b) Once being immersed and aged, there will be electron exchange (shown by the black arrow) and ion exchange (shown by the blue arrow) on the surface of the zinc foil. The zinc ions would be replaced by copper here and diffuse into the solution. Due to the low solubility of ZnF_2 (citation proof), Zn-ions will preferentially combine with fluoride ions and become fluoride precipitates in the outermost layer of the GFA-particles, while the Cu metal would form alloy with the remaining Zn metal.

There are mass increments of 3 different coatings as 0.2 mg cm^{-2}, 0.31 mg cm^{-2}, and 0.36 mg cm^{-2}, respectively, correlated to each side of the GFA-2, 5, 10. It is calculated based on the Zn foil with the size of 5 cm * 5 cm, where the mass increments are originated from the alloyed copper and the newly added zinc fluoride.

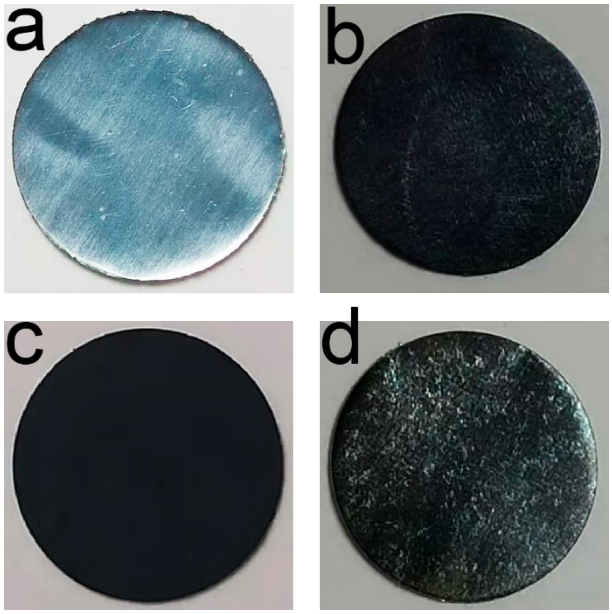

Figure S3. (a)-(d) The optical images of initial state of zinc foil, and the different samples after aging durations, that is, GFA-2, GFA-5, and GFA-10 samples, respectively.

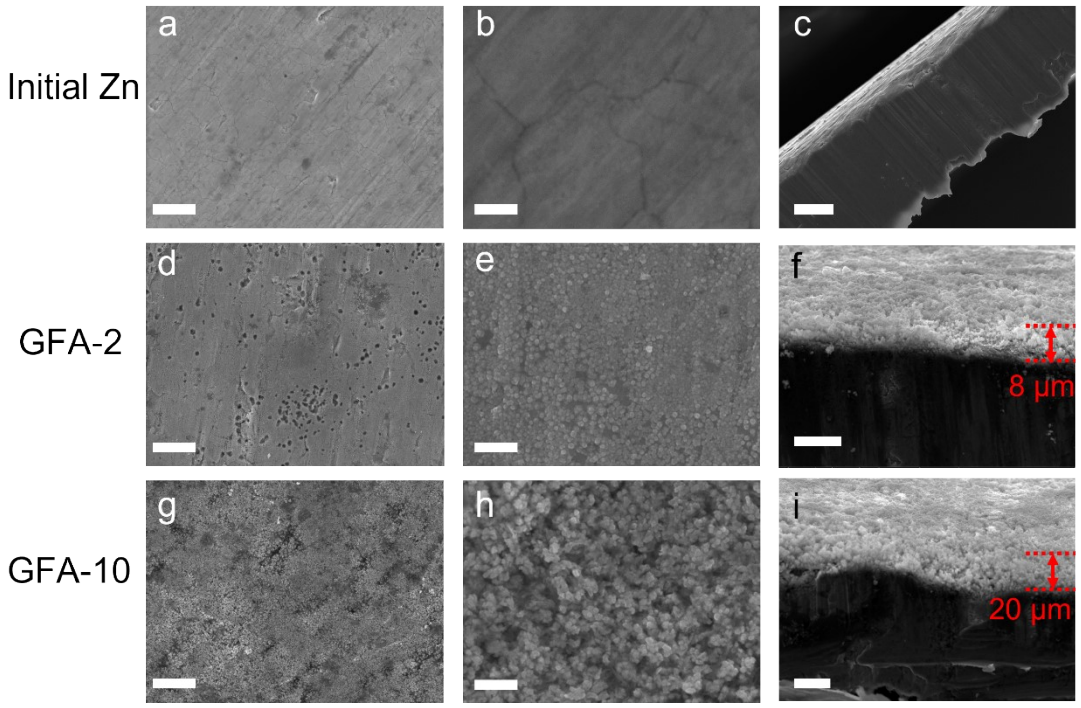

Figure S4. The SEM images of initial states of zinc foil (a)-(c), GFA-2 (d)-(f), GFA-10 (g)-(i), where there are noticeable voids among the GFA nanoparticles for the GFA-2 and GFA-10 samples. The thickness is around 6 μm and 20 μm for GFA-2 and GFA-10 samples, respectively. The scale bars in (a), (c), (d), (g), (i) are 20 μm, in (b), (e), (h) are 2 μm, in (f) is 10 μm.

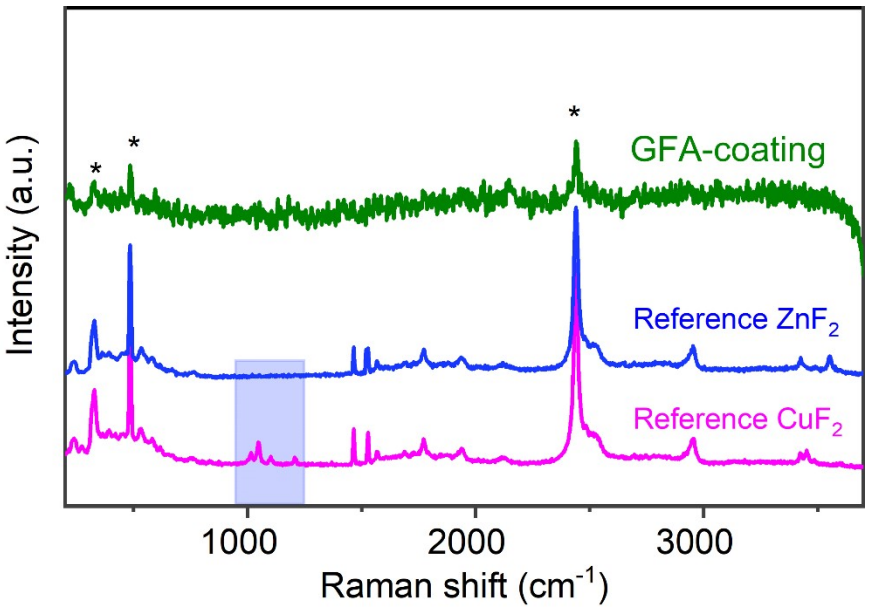

Figure S5. Raman analysis was performed on GFA-coating, and the reference ZnF_2 (Aladdin, Z108925) and CuF_2 (Aladdin, C189213) powders. The finger peaks indicate the presence of fluorides (marked by the asterisk). Of note, the most obvious difference between ZnF_2 and CuF_2 is the peaks between 1000 - 1100 cm^{-1} (1013 cm^{-1}, 1058 cm^{-1}, 1107 cm^{-1}). Even though the GFA-coating did not detect the corresponding peaks (marked by rectangular region) to identify the CuF_2, we cannot rule out the presence of CuF_2 here due to the weak peak intensity. When combining with the results of XRD and TEM results, it can further verify the existence of ZnF_2 at the outmost region of GFA-coating, considering the Raman spectrum detects the outmost surface of the coating.

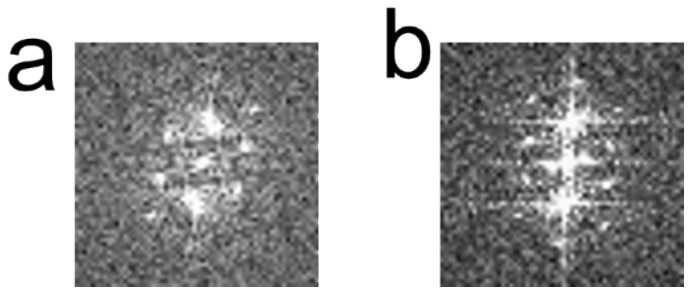

Figure S6. The Fourier transform of TEM image corresponded to the area 1 (a) and area 2 (b) in Figure 1h in main text.

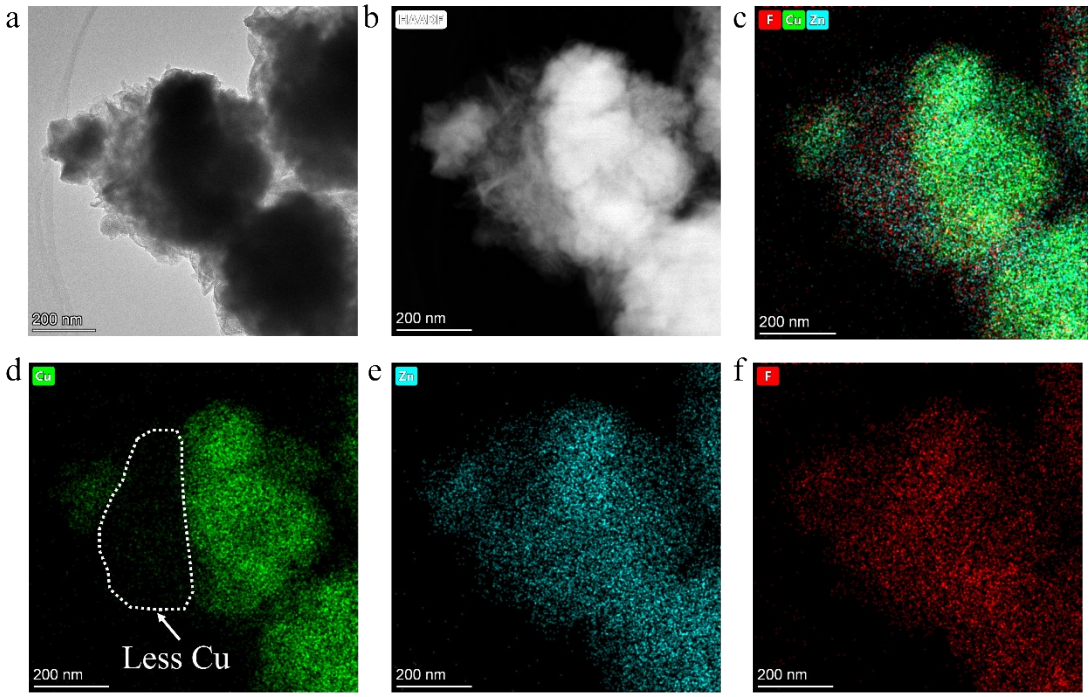

Figure S7. (a) TEM and **(b)** high-angle annular dark-field (HAADF)-STEM images of the biphasic fluorinated alloy nanoparticles with the corresponding EDS mapping for the overlayer **(c)** and the individual Cu **(d)**, Zn **(e)**, and F **(f)** elements. The atomic ratio of Cu element is lesser compared to that of the Zn and F elements of outmost region of the particle, as arrowed out in the Cu distribution image in **(d)**, which is in alignment with the proposed model. All these three detected elements can embody the fluorinated CuZn alloy, which is in accordance with the XPS results to verify the coexistence of F, Zn and Cu elements.

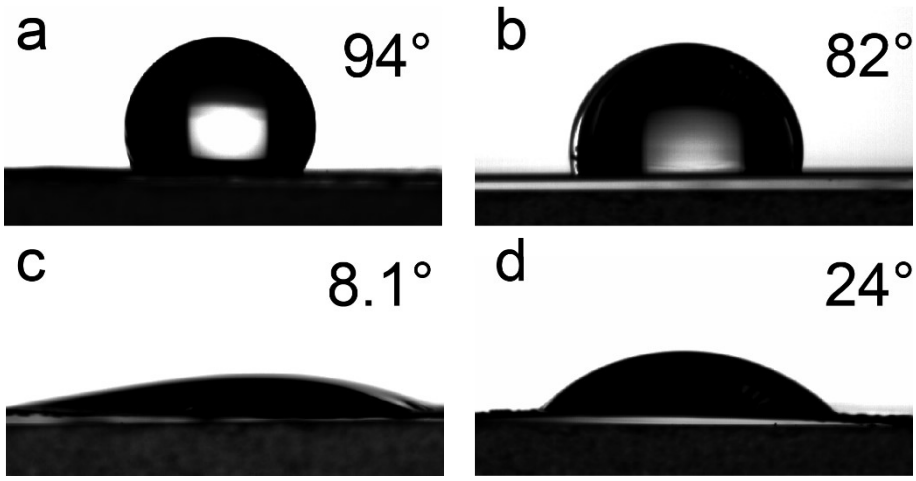

Figure S8. (a)-(d) The contact angle of bare Zn, GFA-2, GFA-5 and GFA-10, respectively.

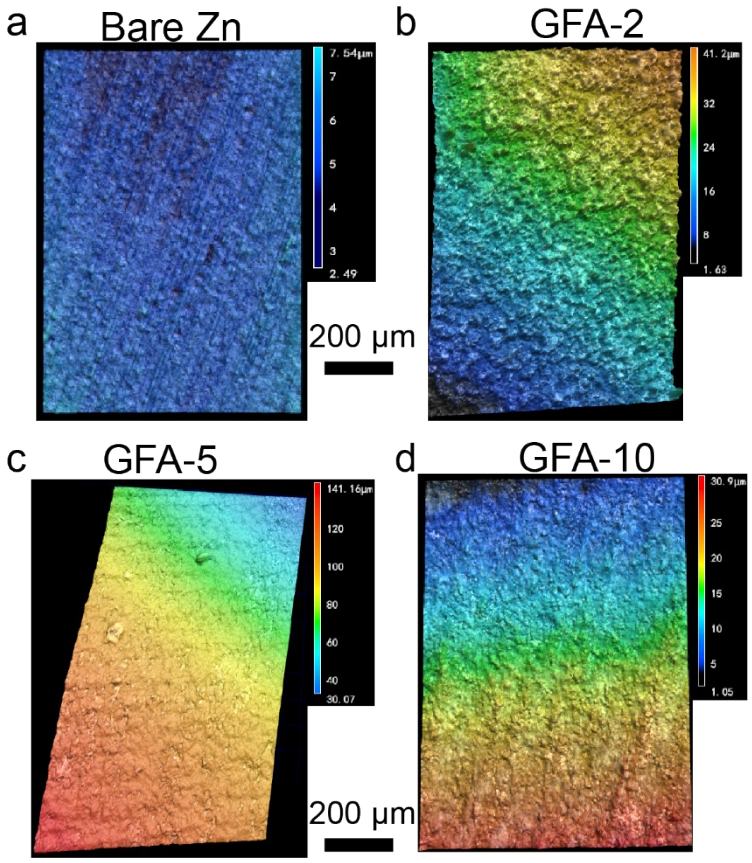

Figure S9. Confocal laser scanning microscope images of different GFA-coated samples to measure the roughness of different states of Zn anodes.

Table S1 The arithmetic mean height of surface roughness parameters were obtained by averaging 5 different areas on the top of different samples corresponded to Figure S7.

Samples / Sz (μm)	Bare Zn	GFA-2	GFA-5	GFA-10
Maximum	3.01	5.63	18.8	9.4
Minimum	1.41	3.41	8.01	5.24
Average	2.31	4.03	11.41	8.16

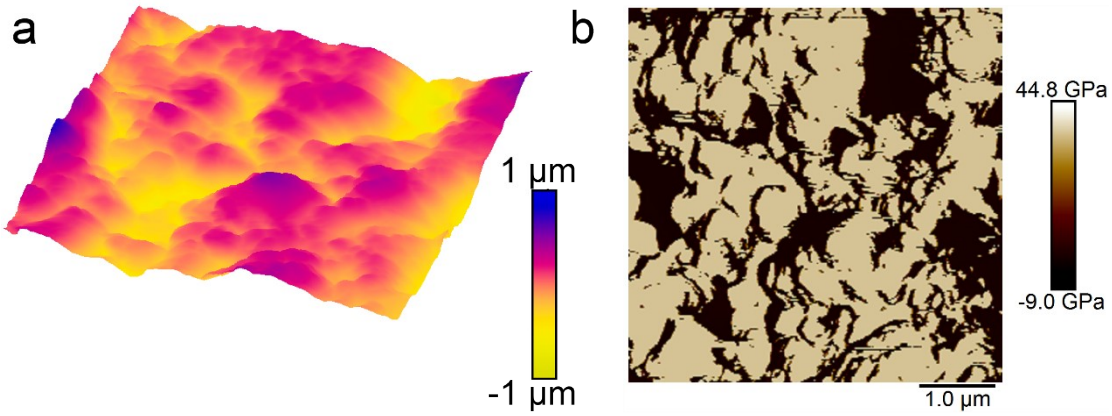

Figure S10. (a) Atomic force microscope image of a GFA-coating to analyze the morphology of GFA-coating with voids. (b) The mechanical properties to analyze the modulus of GFA-coating.

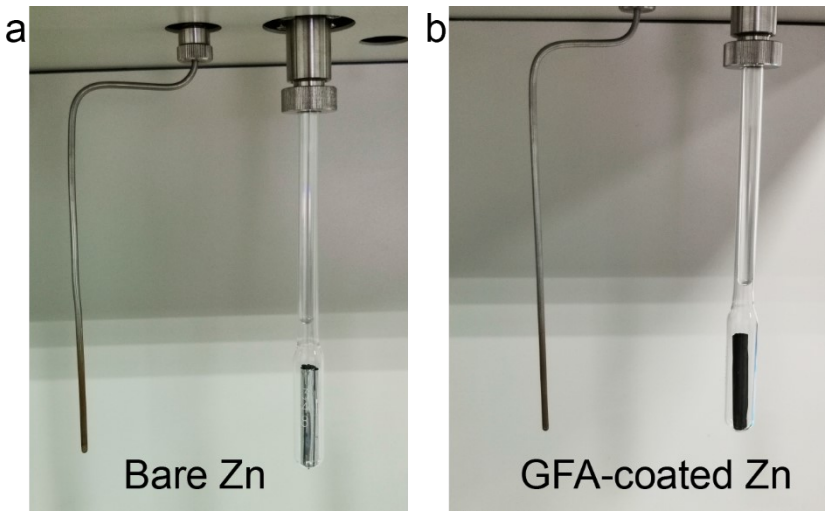

Figure S11. Picture of BET tube to measure the bare Zn (a) and GFA-coated Zn (b), where the size of the measure samples is 25 cm^2, *i.e.*, 5 cm * 5 cm, in curled state.

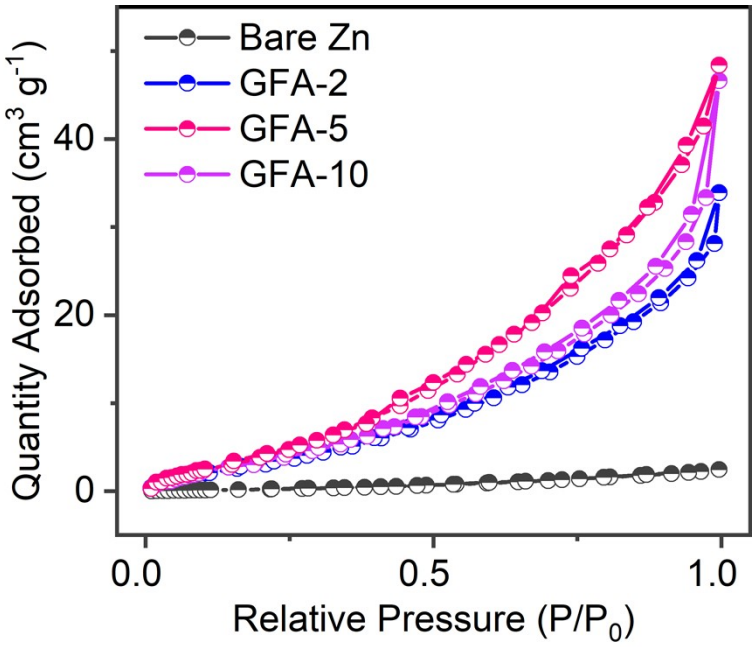

Figure S12. BET results of bare Zn, GFA-2, GFA-5 and GFA-10, respectively. The surface area is 59 cm^2/g for the GFA-2, 124 cm^2/g for the GFA-5 and 117 cm^2/g for GFA-10 samples.

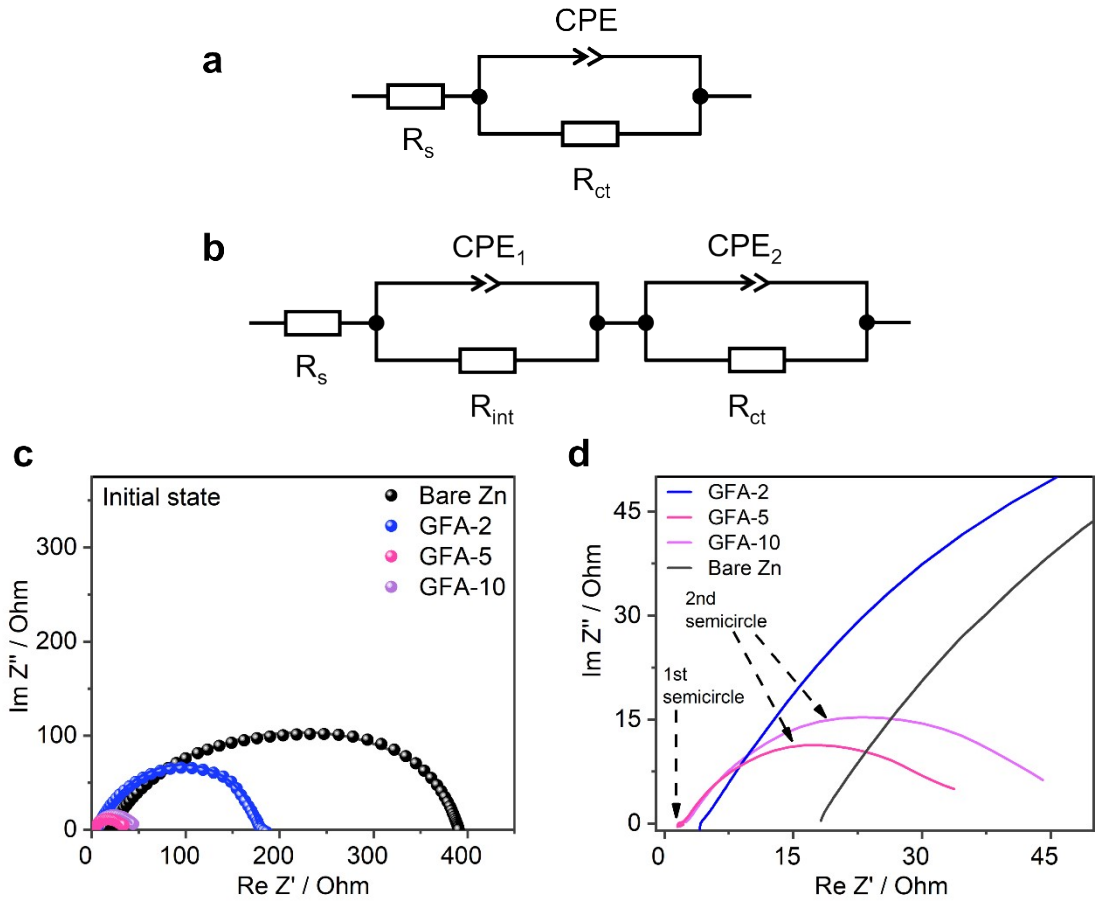

Figure S13. The fitted equivalent circuit for bare Zn (a) and GFA-coated Zn (b). (c) The zoomed-in section of EIS results to determine two semicircles of the GFA-coated Zn, corresponding to Figure 2c in main text.

Table S2 Impedance results of bare Zn anode, and GFA-2, GFA-5 and GFA-10 in symmetric cells corresponded to Figure S10.

Parameters / Samples	R_s (Ω)	R_{int} (Ω)	R_{ct}(Ω)
Bare Zn	17.3		381.3
GFA-2	4.2	140.8	33.1
GFA-5	1.68	0.65	27.4
GFA-10	1.98	0.79	43.4

Supplementary Note 1. Regarding the resistivity of the GFA-coating layer, the voltage response to a direct current of 2 mA was measured for bare Zn foils and GFA-Zn foils, where the electrodes are individually sandwiched between two stainless steel blocking electrodes. Electrical resistivity of GFA-coated Zn electrodes was calculated as following:

$$\rho=(R*S)/L = (U/ I)*(S/L)$$

where the L is the thickness of the coating layer; I – applied current; S- area of the contact between stainless steel and the alloy; U – average voltage increase. For the GFA-5 coating, the total thickness (L) is around 15 μm, the contact area is 1 cm^2. The average voltage increase is 6.1 mV. Thus, the calculated values of electronic resistivity for GFA-coating are $2.1 \cdot 10^4$ Ω·cm.

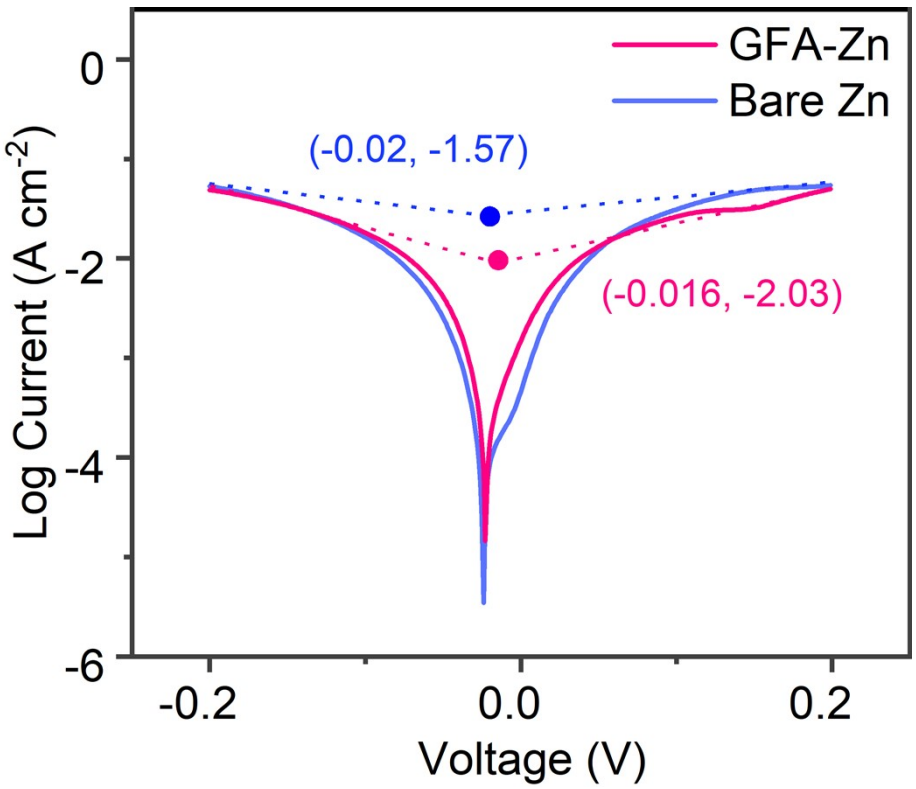

Figure S14. Tafel plots of the symmetric naked Zn and GFA-Zn at a ramp rate of 5 mV/s within the potential range from −0.2 V to +0.2 V versus open circuit voltage (OCV), where the two coordinate points as the corrosion potential and corrosion current are marked out, respectively. The corrosion potential is -0.016 V for GFA-Zn and -0.020 V for the bare Zn electrode, where the more positive corrosion potential of the GFA-Zn correlated to less tendency to corrode. The corresponding corrosion current densities are 10 mA cm^{-2} for GFA-Zn, and 27 mA cm^{-2} for the bare Zn electrode. Larger corrosion current densities indicated the bare Zn was easier to corrode compared to the GFA-Zn. In addition, the cathodic Tafel slope is larger as 126.9 mV dec^{-1} for the GFA-Zn electrode compared to the 78.5 mV dec^{-1} for the bare Zn electrode, indicating a retarded corrosion rate of the GFA-Zn electrode.

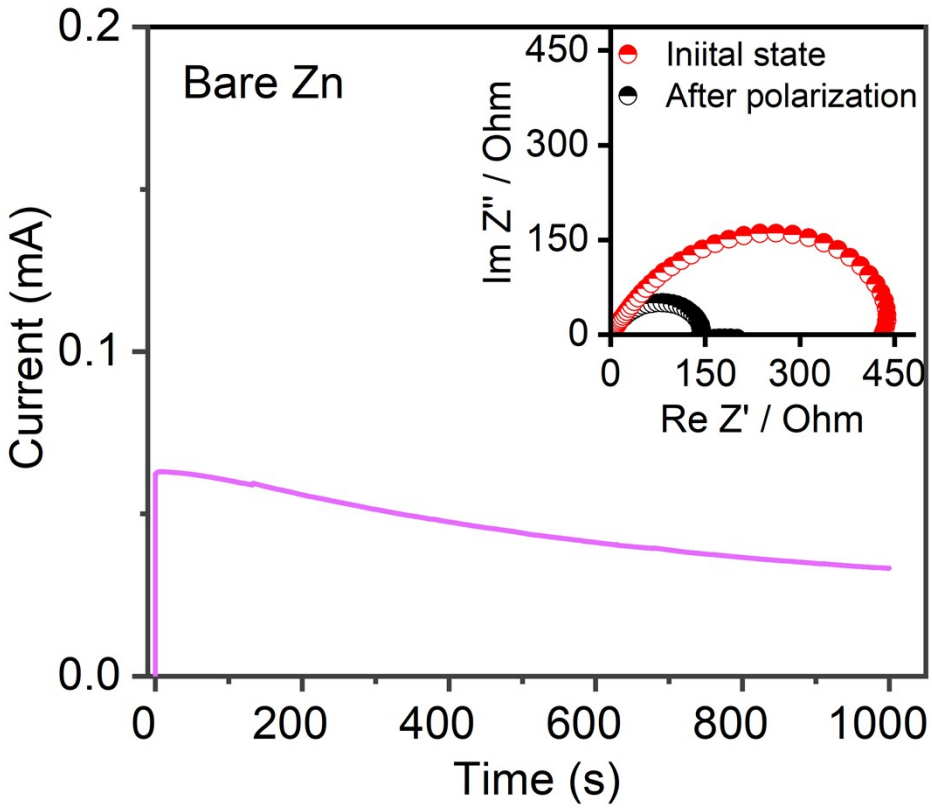

Figure S15. The polarization curve of bare Zn symmetrical cell using chronoamperometry and the inset is the Nyquist plots before and after polarization of bare Zn symmetrical cell.

Supplementary Note 2. Zn^{2+} transference number of the bare GFA-Zn and Zn electrode were evaluated in symmetrical cells by recording the EIS before and after chronoamperometry measurements with applied voltage polarization as 5 mV for 1000 seconds. The transference number is calculated by the following equation:

$$T = \frac{I_s(\Delta V - I_0 R_0)}{I_0(\Delta V - I_s R_s)}$$

where ΔV is the voltage polarization applied, I_0 and R_0 are the initial current and resistance, Is and Rs are the steady state current and resistance, respectively.

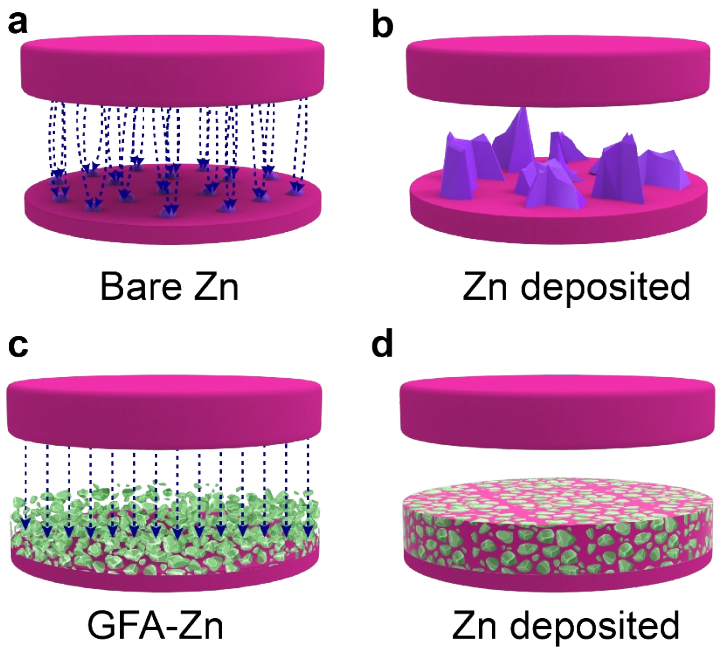

Figure S16. Distribution of the electric field and the different morphologies after zinc deposition in bare and GFA-5 cells, respectively. (a) The electrical field is unevenly distributed by concentrating at microscopically uneven spots, resulting in the dendritic morphology after Zn plating on bare Zn (b). (c) homogenizing the distributions of electrical fields for GFA-Zn electrode, and (d) the void-filling morphology as dendrite-free morphology after Zn plating.

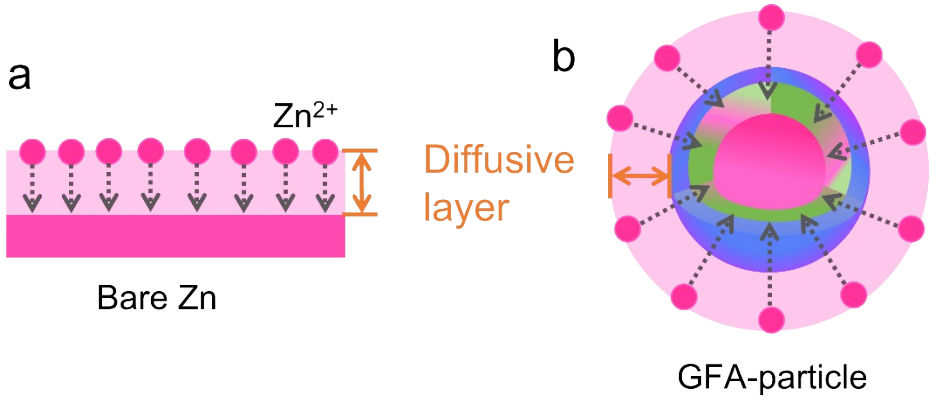

Figure S17. During the Zn deposition process, the diffusion path of Zn-ions from the electrolyte to the electrode surface for different anodes. (a) The vertical diffusion manner for the bare Zn anode, and (b) the 3D spherical diffusion manner for single GFA-particle.

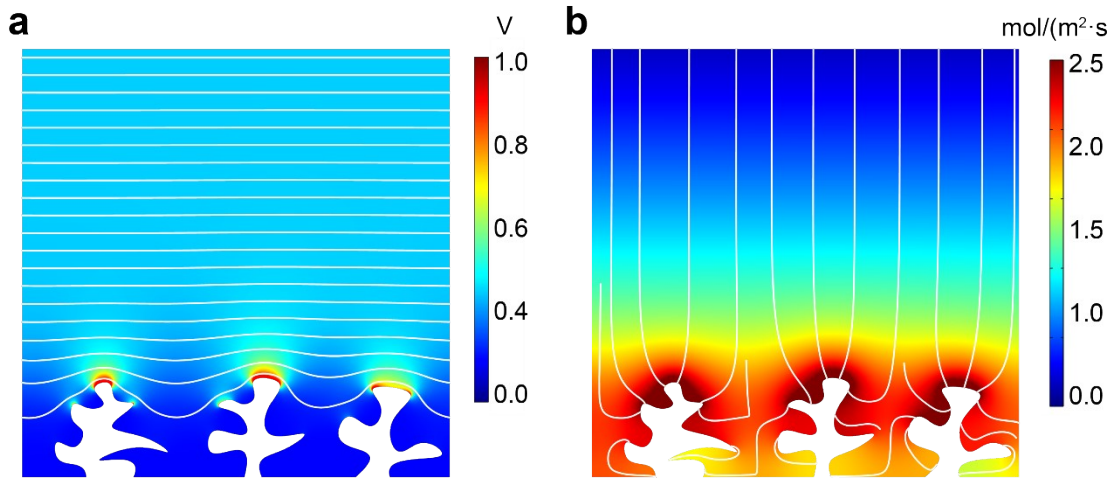

Figure S18. (a) The simulated electric field distribution, and (b) Zn^{2+} ion concentration of bare Zn electrode.

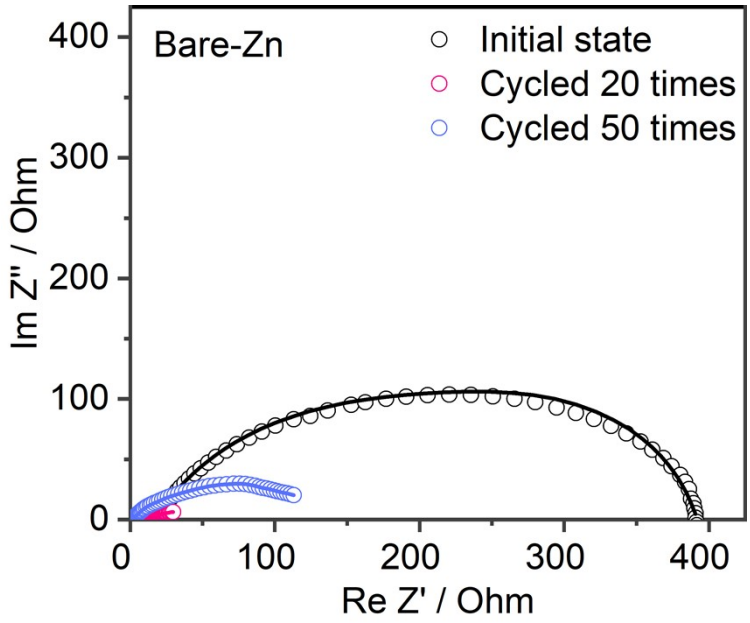

Figure S19. The EIS results for the bare Zn anode in different states and the fitted circuits is used as the above bare Zn case, i.e., Fig. S13a, on the basis of no SEI formed for the interfacial resistance during bare Zn cycling.

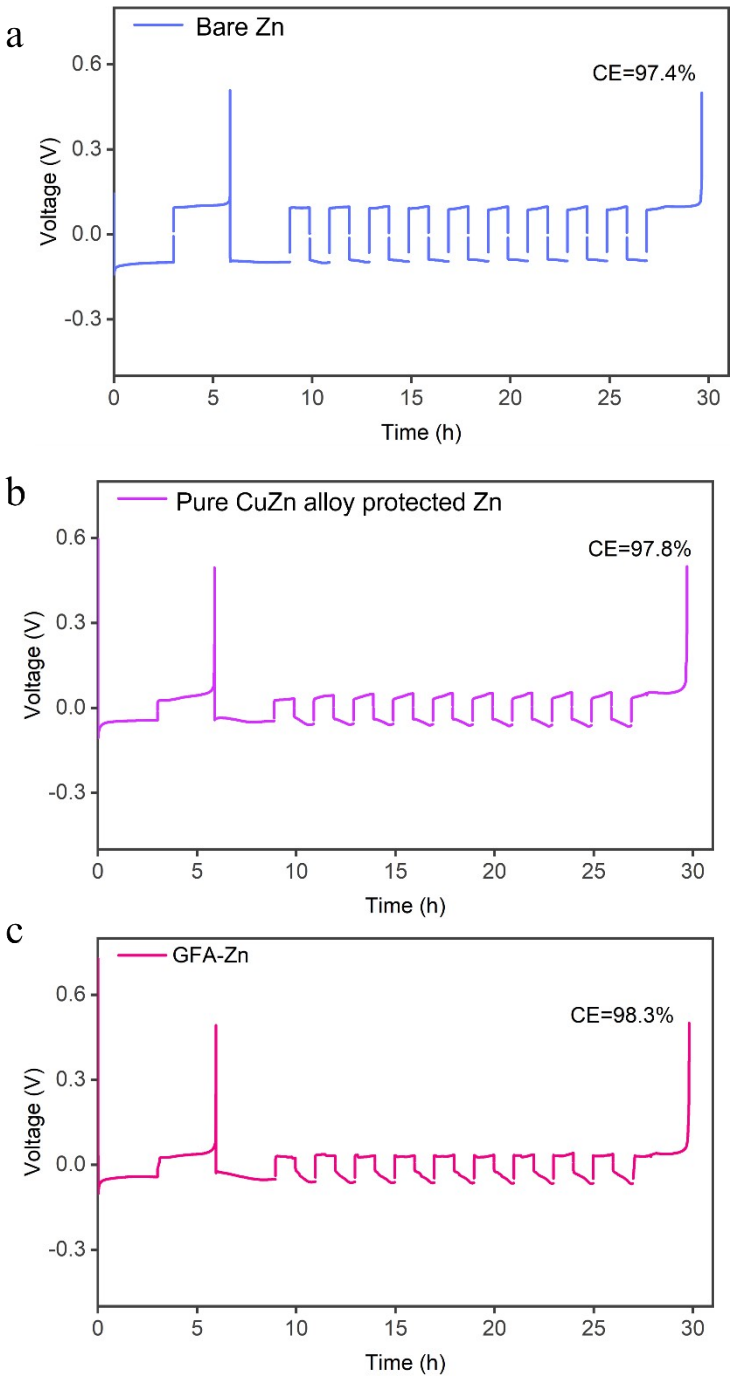

Figure S20. Zn plating/stripping CE tests based on a galvanostatic protocol for different Zn anodes as bare Zn, the pure-CuZn alloy protected Zn, and GFA-Zn. The calculation process of CE is based on the following Note S3. The overpotentials of these three cells recorded at the middle capacity of the 10th plating cycle are 95 mV for the naked Zn electrode, 46 mV for the pure CuZn alloy protected Zn and 35 mV for the GFA-Zn.

Supplementary Note 3. It is galvanostatic protocol evaluate the Zn reversibility to measure the Coulombic Efficiency in asymmetric cells (*Nat. Energy* **5**, 743, 2020). In specific, asymmetric cells as Cu‖Zn cells based on different Zn samples, *i.e.*, bare Zn, pure-CuZn alloy protected Zn, and GFA-Zn, were first conditioned by plating (1 mA cm^{-2}, 3 mAh cm^{-2}) and stripping Zn by charging to 0.5 V during the first cycle. Then, a Zn reservoir was built on the Cu electrode with a capacity of 3 mAh cm^{-2} (Q_t) used for the following cycling. During the following 9 cycles, the current density at 1 mA cm^{-2} was applied for stripping and plating Zn with the capacity of 1mAh cm^{-2} (Q_c) was plated or stripped in each cycle. In the last step, the final capacity (Q_s) was observed when plated Zn was stripped by charging to 0.5 V. The Zn plating/stripping CE were calculated in the equation as:

$$CE=(9Q_c + Q_s)/(9Q_c + Q_t)$$

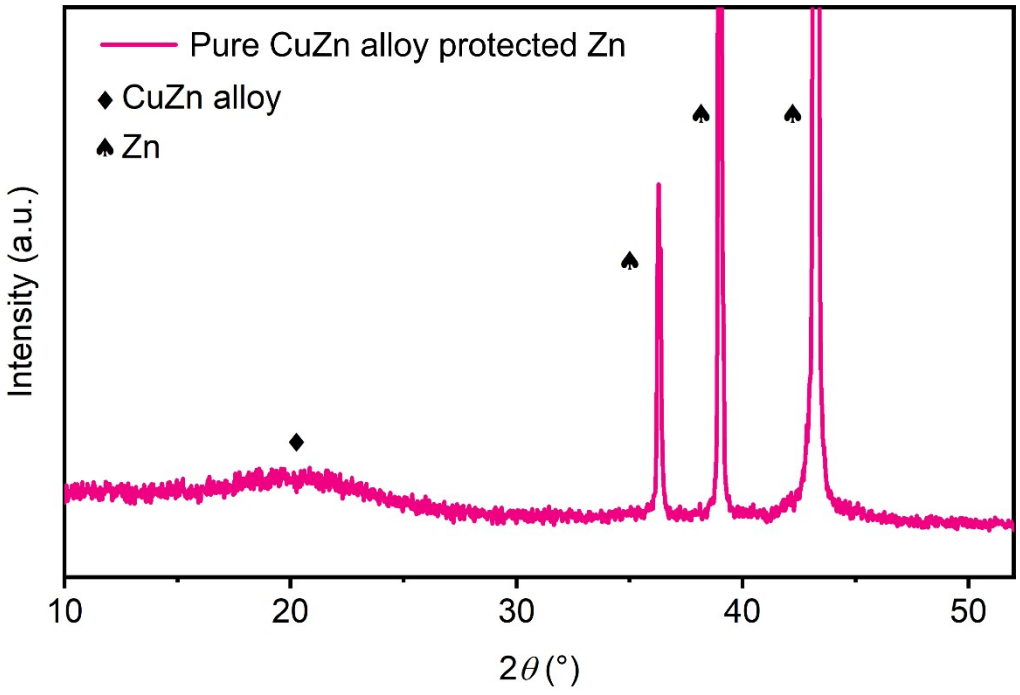

Figure S21. The XRD patterns of pure CuZn alloy-protected Zn metal obtained in 0.01 M $CuCl_2$ solution in the same immersion protocol to prepare the GFA-Zn electrode. Compared with the XRD results of GFA-Zn electrode (Fig. 1a in Main text), one noticeable difference between GFA-Zn and the control sample is the existence of insulating ZnF_2, *i.e.*, the F element, with fingerprint peak at 32.8°

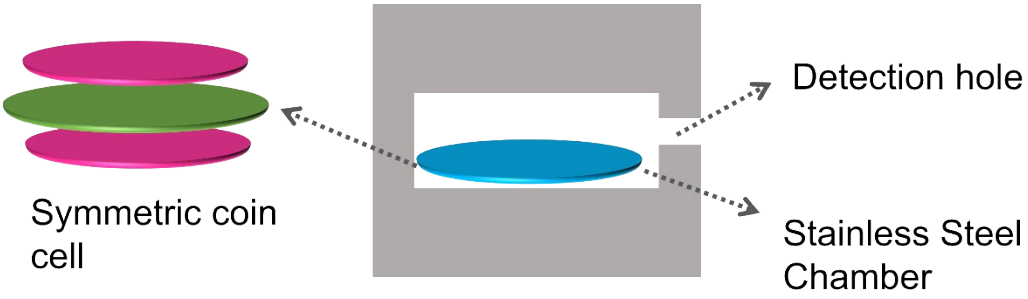

Figure S22. | Cell design of for the online pressure detection of the symmetric cells. The size of the chamber is the 2cm * 2cm * 1cm sized cuboid. There are holes on the coin cell for the gas evaporation into the chamber. The detection hole is used to connect the pressure detector.

Supplementary Note 4. According to the ideal gas law, PV=nRT, where P is the pressure, V is the volume, T is the temperature, n is the molar amount of substance and R is the ideal gas constant. The volume and temperature are maintained constant during Zn deposition, the variations in the chamber pressure can be calculated into the variations in molar amount.

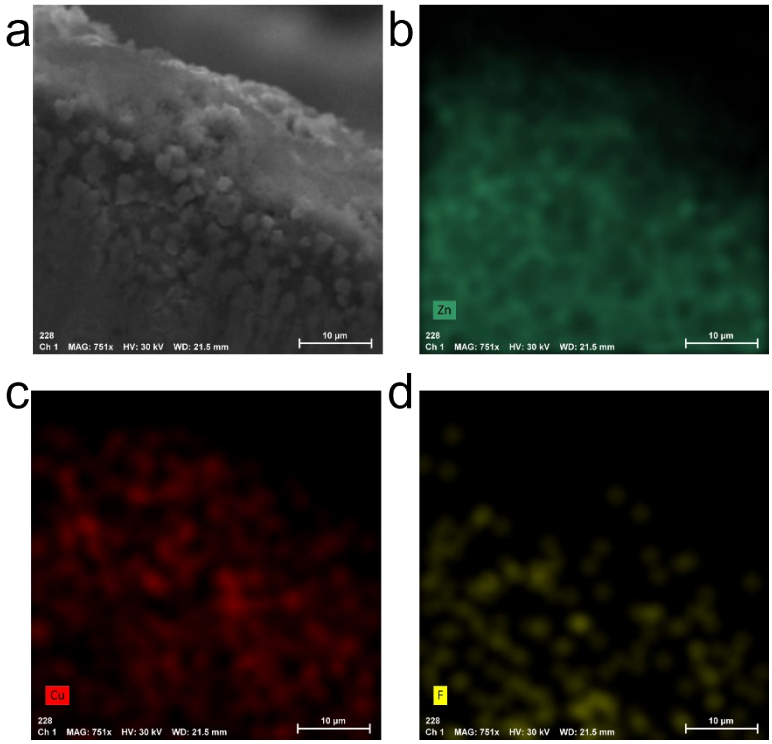

Figure S23. SEM image and corresponding mapping for Zn, Cu, F elements as marked out.

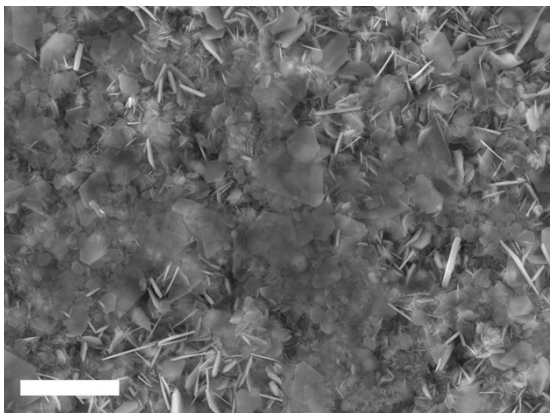

Figure S24. Morphology after depositing larger capacity of 6 mAh cm^{-2}, where the corresponding GFA-5 particles are hardly observed and the electrode surface was covered by typical flake-like deposited Zn. It indicates the voids in the GFA-layer were fulfilled after depositing 6 mAh cm^{-2}.

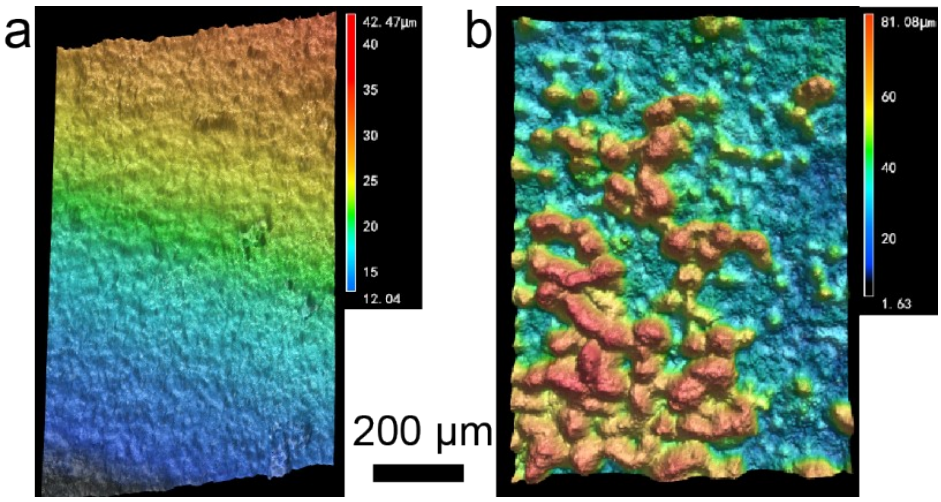

Figure S25. After cycling with designated areal capacity as 3 mAh cm^{-2} for 20 cycles, CLSM images of GFA-Zn (a) and bare Zn (b) in deposited state, corresponding to the surface roughness as 1.7 μm for GFA-Zn and 19.1 μm for bare Zn.

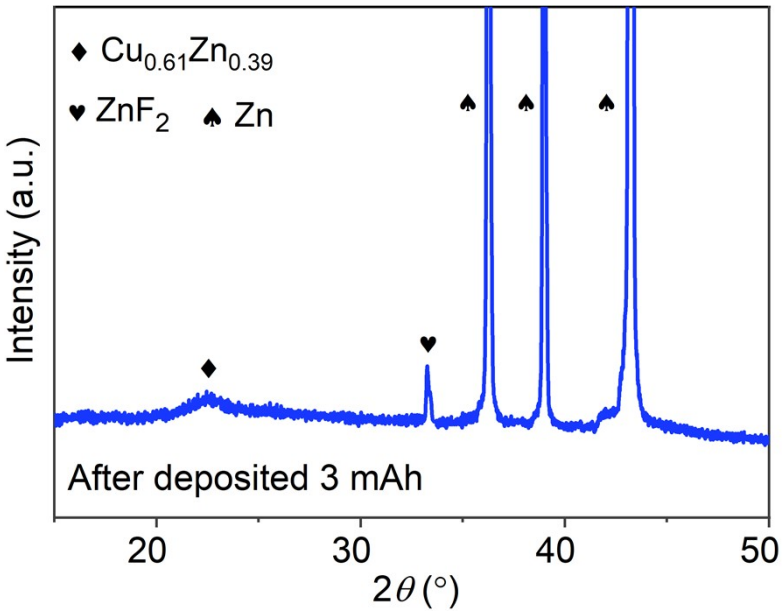

Figure S26. XRD results of the deposited state after plating-stripping with designated areal capacity as 3 mAh cm^{-2} for 20 cycles.

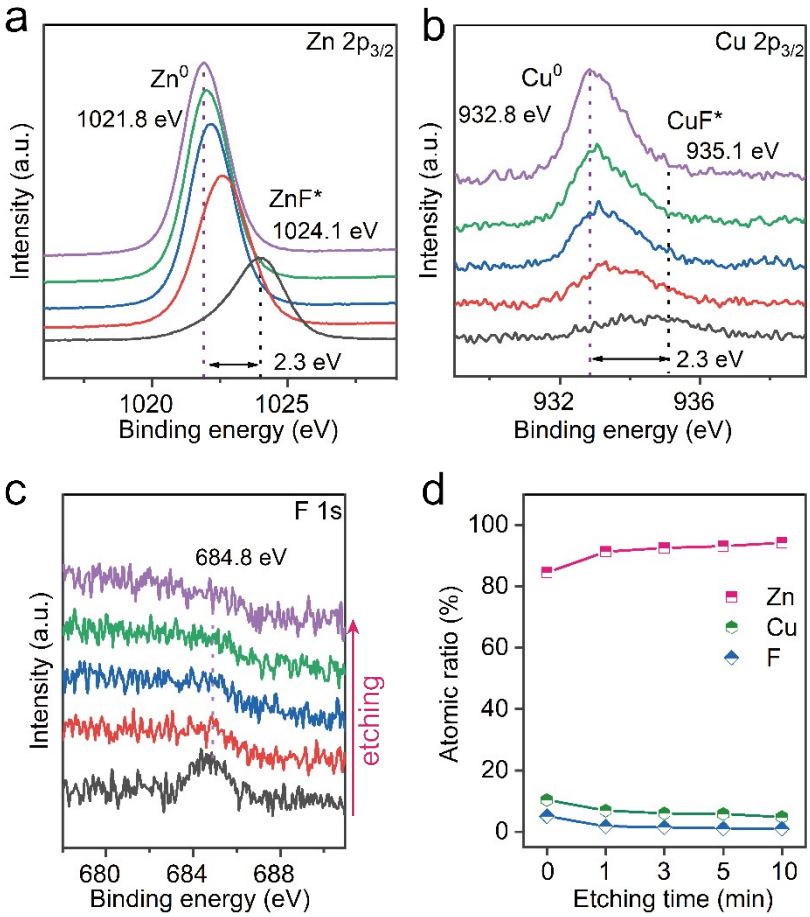

Figure S27. XPS results of the deposited state after cycling with designated areal capacity as 3 mAh cm^{-2} for 20 cycles. The variations in binding energy of Zn is 2.3 eV after etching process of the cycled state, which is larger than the 1.2 eV in initial state (Fig. 1d in main text), while it is smaller of Cu as 2.3 eV in cycled state than the 2.9 eV in initial state. It corresponds to larger variations in valence states of Zn compared to Cu in the GFA-coating, indicating the fluorine atoms became to majorly coordinate with Zn rather than Cu after cycling.

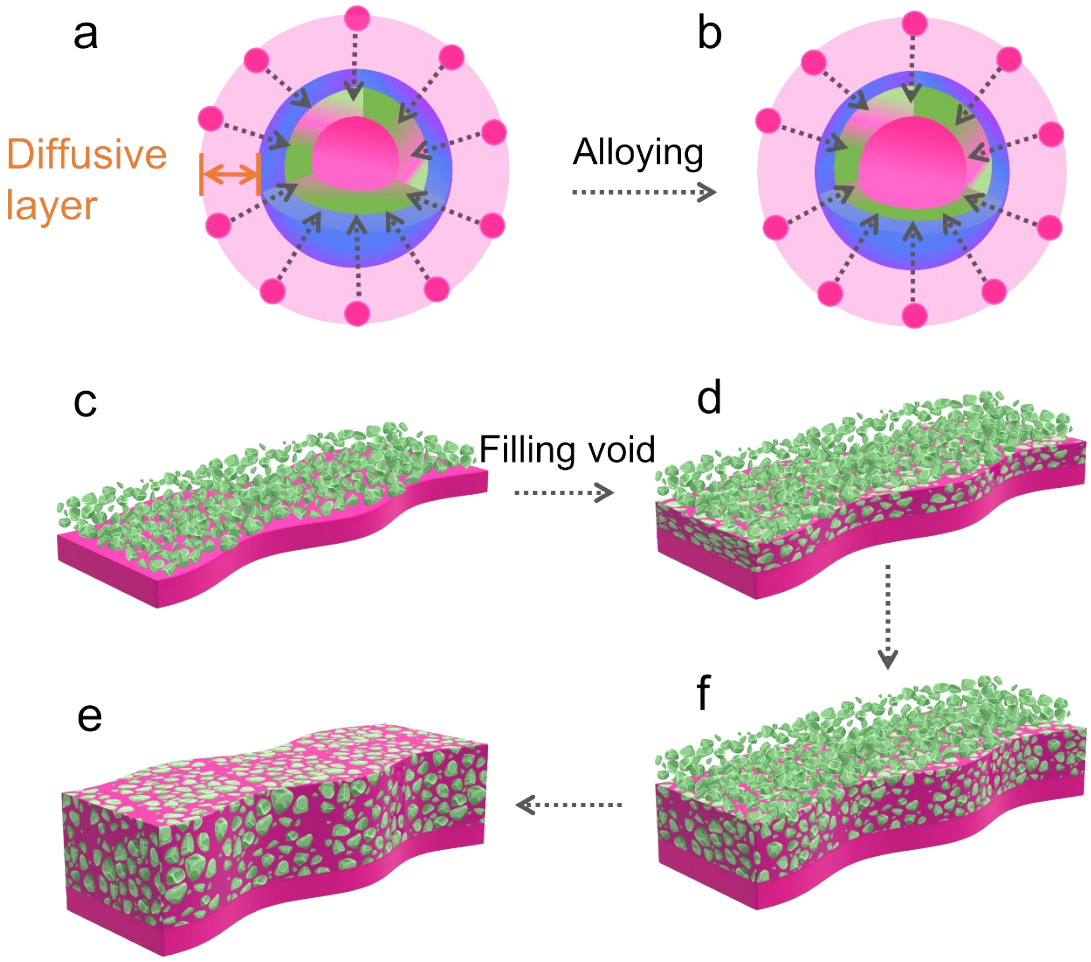

Figure S28. (a)-(b) Illustration of the alloying process of one GFA-particle to store Zn, where the zinc and copper volume inside the GFA-particle will become larger. (c)-(f) Apart from alloying process, the deposited zinc can fill the voids between GFA-particles along Zn deposition.

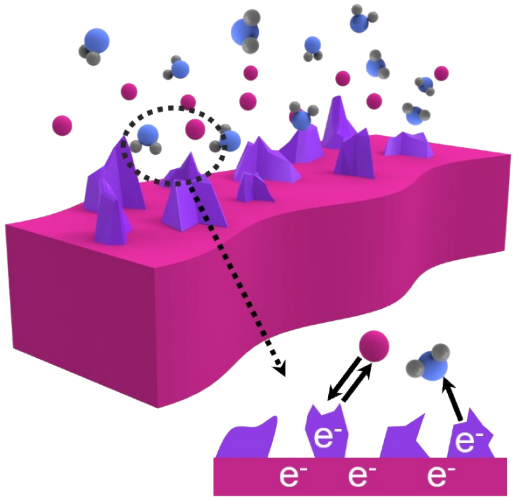

Figure S29. Schematic about Zn-ion transfer and electron flow pathway of Zn deposition process on bare Zn.

Table S3. Performance comparison of the Coating-protected Zn anode based on different coatings.

Coating	Conductive or Insulating	Areal capacity	Cyclic lifetime	Ref.
Nanoporous $CaCO_3$	Insulating	0.05 mAh cm^{-2} at 0.25 mA cm^{-2}	800 h	1
Nanoporous ZnO	Insulating	1.25 mAh cm^{-2} at 5 mA cm^{-2}	500 h	2
Metal-organic framework (MOF)	Insulating	0. 5 mAh cm^{-2} at 0.5 mA cm^{-2}	700 h	3
ZnF_2	Insulating	1 mAh cm^{-2} at 5 mA cm^{-2}	1000 h	4
Faceted TiO_2	Insulating	1 mAh cm^{-2} at 1 mA cm^{-2}	460 h	5
Reduced graphene oxide (r-GO)	Conductive	2 mAh cm^{-2} at 1 mA cm^{-2}	200 h	6
Carbon nanotubes (CNT)	Conductive	0.15 mAh cm^{-2} at 0.5 mA cm^{-2}	400 h	7
MXene	Conductive	0.2 mAh cm^{-2} at 0.2 mA cm^{-2}	800 h	8
GaIn metal	Conductive	0.1 mAh cm^{-2} at 1 mA cm^{-2}	1200 h	9
GFA-5	Conductive + Insulating	1 mAh cm^{-2} at 1 mA cm^{-2}	2000 h	This work
GFA-5	Conductive + Insulating	3 mAh cm^{-2} at 3 mA cm^{-2}	700 h	This work

References for Table S3

1 Kang, L., Cui, M., Jiang, F., Gao, Y., Luo, H., Liu, J., Liang, W. & Zhi, C. Nanoporous CaCO3 Coatings Enabled Uniform Zn Stripping/Plating for Long-Life Zinc Rechargeable Aqueous Batteries. *Advanced Energy Materials* **8**, 1801090 (2018).

2 Xie, X., Liang, S., Gao, J., Guo, S., Guo, J., Wang, C., Xu, G., Wu, X., Chen, G. & Zhou, J. Manipulating the ion-transfer kinetics and interface stability for high-performance zinc metal anodes. *Energy & Environmental Science* **13**, 503-510 (2020).

3 Cao, L., Li, D., Deng, T., Li, Q. & Wang, C. Hydrophobic Organic-Electrolyte-Protected Zinc Anodes for Aqueous Zinc Batteries. *Angewandte Chemie International Edition* **59**, 19292-19296 (2020).

4 Yang, Y., Liu, C., Lv, Z., Yang, H., Zhang, Y., Ye, M., Chen, L., Zhao, J. & Li, C. C. Synergistic Manipulation of Zn2+ Ion Flux and Desolvation Effect Enabled by Anodic Growth of a 3D ZnF2 Matrix for Long-Lifespan and Dendrite-Free Zn Metal Anodes. *Advanced Materials* **33**, 2007388 (2021).

5 Zhang, Q., Luan, J., Huang, X., Wang, Q., Sun, D., Tang, Y., Ji, X. & Wang, H. Revealing the role of crystal orientation of protective layers for stable zinc anode. *Nature Communications* **11**, 3961 (2020).

6 Shen, C., Li, X., Li, N., Xie, K., Wang, J.-g., Liu, X. & Wei, B. Graphene-Boosted, High-Performance Aqueous Zn-Ion Battery. *ACS Applied Materials & Interfaces* **10**, 25446-25453 (2018).

7 Li, M., He, Q., Li, Z., Li, Q., Zhang, Y., Meng, J., Liu, X., Li, S., Wu, B., Chen, L., Liu, Z., Luo, W., Han, C. & Mai, L. A Novel Dendrite-Free Mn2+/Zn2+ Hybrid Battery with 2.3 V Voltage Window and 11000-Cycle Lifespan. *Advanced Energy Materials* **9**, 1901469 (2019).

8 Zhang, N., Huang, S., Yuan, Z., Zhu, J., Zhao, Z. & Niu, Z. Direct Self-Assembly of MXene on Zn Anodes for Dendrite-Free Aqueous Zinc-Ion Batteries. *Angewandte Chemie International Edition* **60**, 2861-2865 (2021).

9 Liu, C., Luo, Z., Deng, W., Wei, W., Chen, L., Pan, A., Ma, J., Wang, C., Zhu, L., Xie, L., Cao, X.-Y., Hu, J., Zou, G., Hou, H. & Ji, X. Liquid Alloy Interlayer for Aqueous Zinc-Ion Battery. *ACS Energy Letters* **6**, 675-683 (2021).

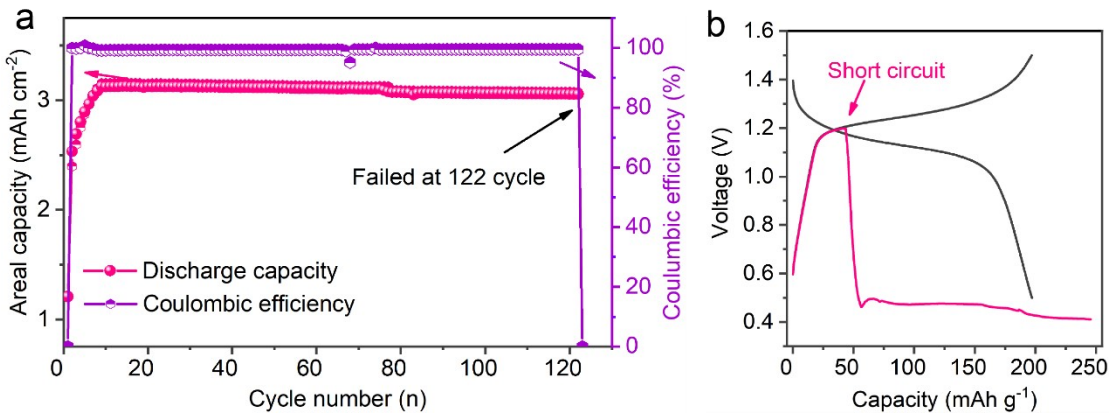

Figure S30. (a) Cycling performance of Zn-I_2 cell based on bare Zn anode, where it suddenly failed after 122 cycles as a premature failure. (b) The charging-discharging voltage profiles of the 121 cycle (black line) and the 122 cycle (pink line), where the voltage dropped down to 0.5 V. Of note, it is a typical phenomenon to diagnose as short circuit with sudden voltage drop in charging process.

Considering it is a sudden failure of Zn-I_2 cells with large areal capacity, showing no gradual capacity decay, it can be resulted from an internal short circuit (>3 mAh cm^{-2}). It is in line with the shorter cyclic stability of bare Zn symmetric cells under the large area capacity (Fig. 3f in main text).